

Numerical accuracy of a Padé-type non-reflecting boundary condition for the finite element solution of acoustic scattering problems at high-frequency

R. Kechroud^{1*}, X. Antoine^{2,3} and A. Soulaïmani¹

¹ *Département de Génie Mécanique, École de Technologie Supérieure,
1100 Notre-Dame Ouest, Montréal (Québec), H3C 1K3, Canada.
E-mail: {kechroud.riyad, azzeddine.soulaïmani}@etsmtl.ca*

² *Laboratoire de Mathématiques pour l'Industrie et la Physique, UMR 5640, UFR MIG,
Université P. Sabatier, 118, route de Narbonne, 31062 Toulouse Cedex, France.
E-mail: antoine@mip.ups-tlse.fr*

³ *Applied and Computational Mathematics, Division of Engineering and Applied Sciences,
California Institute of Technology, 1200 E. California Blvd, 207-50, Pasadena, CA 91125, USA.
E-mail: antoine@acm.caltech.edu*

SUMMARY

The present text deals with the numerical solution of two-dimensional high-frequency acoustic scattering problems using a new high-order and asymptotic Padé-type artificial boundary condition. The Padé-type condition is easy-to-implement in a Galerkin Least-Squares (iterative) finite element solver for arbitrarily convex-shaped boundaries. The method accuracy is investigated for different model problems and for the scattering problem by a submarine-shaped scatterer. As a result, relatively small computational domains optimized according to the shape of the scatterer can be considered while yielding accurate computations for high frequencies. Copyright © 2000 John Wiley & Sons, Ltd.

1. INTRODUCTION

The numerical solution of acoustic scattering problems in the high-frequency spectrum, and for large targets, remains one of the most challenging issues in scientific computing [1]. Two major difficulties characterize these problems: the first difficulty is linked to *the unboundedness of the computational domain* and the second difficulty involves *a small asymptotic parameter*, the wavelength of the incident field compared to the characteristic size of the scatterer. Different numerical techniques, such as the boundary element methods [2, 3, 4, 5, 6, 7], the finite element methods [8, 9, 10, 11, 12, 13, 14, 15, 16, 17, 18], the infinite element methods [19], are available to solve these problems. However, the difficulties of simulation need to be further investigated to increase the accuracy of the computed solution and/or the frequency of the incident

*Correspondence to: R. Kechroud, Département de Génie Mécanique, École de Technologie Supérieure; 1100 Notre-Dame Ouest, Montréal (Québec), H3C 1K3, Canada; E-mail: Kechroud.Riyad@etsmtl.ca

†This research has been funded by the National Sciences and Engineering Research Council of Canada (NSERC).

signal. Indeed, these two important practical issues generally require fine discretization grids associated to small spatial discretization steps. As a result, the solution of a large and highly indefinite linear system is generally required by means of an iterative solver [6, 10, 11, 17, 20].

Among all these improvements, the construction of accurate local approximate truncation boundary conditions defined on general-shaped and optimized fictitious boundaries is of utmost importance in computational acoustics. Since the pioneering work of Engquist and Majda [21] and Bayliss *et al.* [12, 13], numerous developments and improvements have been achieved [10, 11, 14, 15, 16, 17, 18, 22, 24] but the possibility of considering high frequencies still remains challenging. In a series of recent papers [10, 11, 25, 26, 27], it has been shown that the Bayliss-Gunzburger-Turkel-like (BGT-like) Absorbing Boundary Condition (ABC) developed in [24] yields efficient and flexible iterative finite element solvers [10, 11, 28] which allow the handling of complex scattering configurations. This ABC has the interesting feature of being easy-to-implement in a finite element formulation for general arbitrarily-shaped two- and three-dimensional fictitious boundaries. The possibility of choosing a general fictitious boundary is an extremely important issue in the development of codes since it is the essential problem in the reduction of the computational domain. The general fictitious boundaries are important and are often met in practice if one considers an elongated scatterer, for example a three-dimensional submarine in computational acoustics (similar situations and questions occur for the full set of Maxwell's equations in computational electromagnetism). However, even if the BGT-like ABC is flexible [10, 11], the solution to a scattering problem in the high frequency domain requires one to take into account higher harmonics in the scattered field [22, 29]. The BGT-like radiation boundary condition, which accurately models the first propagative modes, needs to be placed at a larger distance from the scatterer if one wishes to preserve an accurate computation. As a result, the involvement of a large size computational domain is required leading to stronger pollution effects in a Galerkin finite element method. Fine discretization meshes are therefore needed and lead to the resolution of very large scale indefinite linear systems.

A very promising research direction relies on the development of higher-order non-reflecting boundary conditions [30, 31, 32]. In the recent review paper by Givoli [30], the author emphasizes the fact that high-order Padé-type non-reflecting boundary conditions are useful require the involvement of only a few additional (partial) differential equations on the fictitious surface for a nontrivial improvement of accuracy. Moreover, these equations are second-order with respect to the tangential derivatives and hence do not need the consideration of high-order finite element methods (linear being sufficient). Furthermore, the equations being of differential type, they lead to sparse matrix representations in a finite element (or finite difference) context preserving the properties of the volumetric formulation associated with the Helmholtz equation. The first class of non-reflecting boundary operators are the exact operators. Unfortunately, to the best of the authors' knowledge, these exact operators are only available for specific simple shapes: half-plane, rectangles (by adding the suitable corner's conditions of Collino), circle and sphere. This restriction to simple shapes is a serious bottleneck if we wish to solve scattering problems by elongated scatterers. Indeed, only having simple shapes at our disposal for the ABC directly contradicts our desire to choose a smooth arbitrarily-shaped fictitious boundary to reduce the computational domain. In our opinion, a compromise has to be reached. Indeed, it seems that we must choose between

- an exact boundary condition given for a special simple shape but no optimized

computational domain

- and the possibility of considering general shapes but with an approximate (and asymptotic in a certain way) high-order boundary condition to optimize the computational domain for an elongated scatterer (and, incidentally, also to reduce the pollution in the finite element method).

We propose to investigate the second direction in view of the solution of high-frequency scattering problems for engineering calculations.

Our basic philosophy is to produce a high-order Padé-type BGT-like radiation condition for a general shape. The initial work of Bayliss *et al.* has been based on the development of a series of differential operators with the goal to annihilate the first terms of the high-frequency asymptotic expansion of the scattered field. Fundamentally, this approach makes the restrictive assumption that the scattered field admits an *a priori* Ansatz as a series in inverse integer powers of the wavenumber. This Ansatz is surely true if one considers that we are in the far-field zone but fails if we assume that we are in the near-field region. Indeed, as predicted by the general theory of diffraction, fractional terms (like $k^{-1/3}$) should be involved in the *a priori* near-field Ansatz of the diffracted field. If one expects to build an efficient extension of the BGT-like ABC, which can also be applied in the near-field zone in order to reduce the computational domain, then the annihilation operators should incorporate fractional powers of the wavenumber. In the initial paper about the derivation of the BGT-like ABC [24], the classical calculus of pseudodifferential operators has been used to extend the original BGT condition to the BGT-like ABC used in [10, 11]. Once again, this classical calculus assumes that we only consider integer powers of the wavenumber. This explains the singularity which appears in the principal symbol of the approximate non-reflecting boundary operator yielding the BGT conditions and which induces some errors in the approximation of the exact Dirichlet-to-Neumann map near the (local) cut-off frequencies. A detailed and formal study has been developed in [22] which emphasizes these problems and proposes an alternative solution to increase the accuracy of the BGT-like ABC using a new smooth principal symbol for the approximation of the exact DtN map for an arbitrarily shaped scatterer. It is shown in [22] that this new operator is quite efficient and accurate in the On-Surface Radiation Condition (OSRC) context [28, 34] and most particularly in the high-frequency spectrum. This condition is also easy-to-use in a finite element code. Finally, the efficient extensions to both the three-dimensional acoustic and electromagnetism are given in [40]. We propose here to numerically investigate its capability as an ABC to consider a small computational domain while remaining accurate (for far-field calculations for instance) in the high-frequency regime. We will also emphasize the fact that this new condition only requires a small changes to a basic finite element solver.

The plan of the paper is as follows. In Section 2, we recall some basic results concerning the sound-hard scattering problem and the BGT-like ABC. In Section 3, we introduce the Padé-type ABC and its formulation using some auxiliary surface functions. We explain the main features and properties of this condition and describe the main issues concerning its derivation. Section 4 concerns a possible (and non-unique) associated coupled variational formulation, its Galerkin Least-Squares finite element approximation (see [8, 9] for instance) and its implementation in a preconditioned ILUT iterative GMRES solver [17, 20]. (Note that at this step, our goal is restricted to analyze the improvement induced by the new ABC in terms of mesh reduction and *not* to propose a high-performance iterative solver.

Further developments still need to be realized essentially with respect to the preconditioning techniques. These implementation details are given to show that only small adaptations are required. We furthermore emphasize some difficult questions related to the new conditions, essentially, the solution to the associated linear system and the related choice of the variational formulations.) Section 5 deals with some first experiments concerning the behavior of the new ABC for different models of scatterers and general fictitious shapes. In Section 6, we analyze its performance to solve the scattering problem by a submarine-shaped scatterer. In the last section, we discuss the conclusion and propose some possible directions and extensions.

2. EXACT AND APPROXIMATE MATHEMATICAL MODELS

2.1. The two-dimensional exterior acoustic scattering problem

Let us define Ω^- as a two-dimensional bounded scatterer with boundary Γ . We denote by Ω^{ext} the associated exterior domain of propagation. Then, the scattering of an incident time-harmonic acoustic wave u^{inc} by an impenetrable scatterer Ω^- embedded in a homogeneous medium Ω^{ext} can be formulated as the following exterior boundary value problem (BVP) [2, 7]: find the scattered field u such that

$$\begin{cases} \Delta u + k^2 u = 0, & \text{in } \Omega^{\text{ext}}, \\ u = g = -u^{\text{inc}} \text{ or } \partial_{\mathbf{n}_\Gamma} u = g = -\partial_{\mathbf{n}_\Gamma} u^{\text{inc}}, & \text{on } \Gamma, \\ \lim_{|x| \rightarrow \infty} |x|^{1/2} (\nabla u \cdot \frac{x}{|x|} - iku) = 0. \end{cases} \quad (1)$$

The operator $\Delta = \sum_{j=1}^2 \partial_{x_j}^2$ designates the usual Laplacian operator in Cartesian coordinates and $(\Delta + k^2)$ is the well-known Helmholtz operator. The real positive number k is the wave number in the unbounded domain Ω^{ext} . This parameter is related to the wavelength λ of the incident signal by the relation $k = 2\pi/\lambda$. In the sequel, we consider an incident plane wave $u^{\text{inc}}(x) = e^{ik\mathbf{x} \cdot \mathbf{d}}$, where $\mathbf{d} = (\cos(\theta^{\text{inc}}), \sin(\theta^{\text{inc}}))^T$ is the normalized incidence vector in the polar coordinate system. The boundary conditions respectively model the classical sound-soft (Dirichlet) or sound-hard (Neumann) scattering problem for a datum g expressed in terms of incident field, denoting by \mathbf{n}_Γ the outward unitary normal vector to Ω^- at the boundary Γ . Finally, the last relation is the well-known Sommerfeld radiation condition which yields the uniqueness of the solution to the BVP and the positiveness of the energy flux.

2.2. Formulation in a bounded domain with the local second-order BGT-like non-reflecting boundary condition

The solution to the above BVP can be obtained by truncating the exterior domain of propagation by a fictitious boundary Σ which surrounds the scatterer. For numerical purposes, one crucial choice consists of selecting a suitable *local* boundary condition on Σ to reduce the computational domain Ω of boundary $\Gamma \cup \Sigma$ without generating spurious reflections at the boundary. Such a condition is often called an *Artificial* or a *non-reflecting* Boundary Condition (ABC). We refer to [15, 16, 18, 30] for a survey on the techniques of ABCs. Several methods for designing such conditions are available.

It has recently been shown by Farhat *et al.* [10, 11, 25, 26, 27] that the second-order Bayliss-Gunzburger-Turkel-like (BGT) radiation condition derived in [24] yields some efficient finite

element calculations for two- and three-dimensional direct and inverse acoustic scattering problems for arbitrarily-shaped fictitious surfaces. For the sake of conciseness, we propose to only consider the sound-hard scattering problem, since the extension to the sound-soft scattering problem is straightforward. The approximate truncated BVP with the second-order BGT-like radiation condition [24] is set as

$$\begin{cases} \Delta u + k^2 u = 0, & \text{in } \Omega, \\ \partial_{\mathbf{n}_\Gamma} u = g, & \text{on } \Gamma, \\ \partial_{\mathbf{n}_\Sigma} u = -M_2 u & \text{on } \Sigma, \end{cases} \quad (2)$$

where the unit normal vector \mathbf{n}_Σ to Σ is inwardly directed to Ω . For brevity, we denote by u the approximate scattered field solution to the BVP (2). The last equation of system (2) defines an ABC on the general fictitious boundary Σ which is assumed to be convex. In [24], this condition is built as a second-order Taylor expansion of the Dirichlet-to-Neumann (DtN) operator. We recall this process in the next subsection to compare the improvements of the new ABC with the usual BGT-like ABC. In two dimensions, the resulting symmetrical differential operator M_2 is defined by

$$-M_2 u = iku - \frac{\kappa}{2} u + \frac{\kappa^2}{8(\kappa - ik)} u + \partial_s \left(\frac{1}{2(\kappa - ik)} \partial_s u \right) \quad (3)$$

where s is the counterclockwise directed arclength over Σ and $\kappa = \kappa(s)$ is the curvature at this point.

For the finite element approximation, the curvature is approximated by the following scheme: let $K = (ABC)$ be a triangle with vertices A , B and C on Σ_h (the discrete polygonal interpolated fictitious boundary), then the curvature can be accurately approximated at point B by

$$\kappa(B) \simeq \frac{4 \text{area}(K)}{abc}.$$

Real numbers a , b and c are the different side lengths of K satisfying $a \geq b \geq c$. The area of K is evaluated by the stable formula

$$\text{area}(K) = \frac{\sqrt{(a + (b + c))(a + (b - c))(c + (a - b))(c - (a - b))}}{4}.$$

In the case of boundaries with curvature discontinuities, as for example for a rectangle, this numerical curvature has proven to be efficient [28, 33].

Even if this condition is accurate in the medium frequency range [10, 11], its precision decreases in the high-frequency regime if the fictitious boundary is too close to the scatterer. To obtain suitable calculations, a larger computational domain must be considered. As explained in details in the introduction, this leads to the solution of very large-size sparse linear systems which are computationally expensive both in memory and time, even with sophisticated solvers (see for instance the FETI-H method used in [11] for three-dimensional calculations). As a result, this is a significant limitation to the investigation of high-frequency direct scattering problems.

3. A HIGH-ORDER PADE-TYPE ABC FOR HIGH-FREQUENCY SCATTERING

In a recent work [22], a modification to the second-order BGT-like ABC has been proposed in the On-Surface Radiation Condition (OSRC) context [28, 33, 34]. The new radiation condition takes the following form

$$\partial_{\mathbf{n}_\Sigma} u = ik \sqrt{1 + \partial_s \left(\frac{1}{k_\epsilon^2} \partial_s \right)} u - \frac{\kappa}{2} u + \frac{\kappa^2}{8(\kappa - ik)} u - \partial_s \left(\frac{\kappa}{2k^2} \partial_s u \right), \quad (4)$$

setting $k_\epsilon = k + i\epsilon$ as a new damped complex wave number. The ϵ damping parameter is optimized in [22] as explained below and is related to both the frequency and curvature by $\epsilon = 0.4k^{1/3}\kappa^{2/3}$. In the sequel, \sqrt{z} designates the principal determination of the square-root of a complex number z with branch-cut along the negative real axis.

Let us emphasize the different original points concerning the derivation of this condition (see [22] for more details). The first idea consists of locally mapping a neighborhood of a point on the surface to an open neighborhood of the half-plane using patches. The local portion of the exterior (respectively interior) space is mapped to the right (respectively left) half-plane, the part of the fictitious boundary coincides locally with the half-plane $\{x = 0\}$. Using the techniques of classical pseudodifferential calculus, the principal (classical and homogeneous) symbol λ_1 [35] to the exterior Dirichlet-to-Neumann (DtN) map can be computed. Essentially, this term is

$$\lambda_1 = ik \sqrt{1 - \frac{|\xi|^2}{k^2}}, \quad (5)$$

where ξ is the covariable by Fourier transform of s by mapping. For example, if one considers the symbol $\sigma(P) = -|\xi|^2$, the corresponding operator P is the Laplace-Beltrami operator $P = \Delta_\Sigma = \partial_s^2$ over the surface Σ . This means that, in terms of operator, we have a first approximation of the DtN map by a truncation of its *a priori* infinite (and unfortunately non-uniform) symbolical asymptotic expansion in homogeneous symbols. A higher-order approximation is

$$\text{DtN} \approx \Lambda_{2-j} = \text{Op} \left(\sum_{l=j}^1 \lambda_l \right) \quad (6)$$

taking into account the first $(2-j)$ terms. The notation $\text{Op}(\sigma)$ designates the operator given by inverse Fourier transform through the symbol σ . Let us now refer back to the equation (5). This operator is accurate if it is set on a straight boundary but becomes inaccurate for a curved boundary (a circle for example [22]). More precisely, its singularity for frequencies $|\xi| \approx k$ implies that it does not model correctly the harmonics near the cut-off frequencies. These harmonics correspond to tangential modes which must be well-modelled as shown in [22, 29] if one expects to have a fictitious boundary Σ closer to the physical boundary Γ , more particularly for high-frequencies. To realize this goal, the solution proposed in [22] consists of locally regularizing the symbol λ_1 as

$$\lambda_{1,\epsilon} = ik \sqrt{1 - \frac{|\xi|^2}{k_\epsilon^2}}, \quad (7)$$

with $k_\epsilon = k + i\epsilon$. The parameter ϵ is chosen so that it minimizes the reflection coefficient associated to the tangential modes for the circular cylinder of radius R . The estimate of this

coefficient yields an nearly optimal parameter ϵ as: $\epsilon = 0.4k^{1/3}R^{-2/3}$. The associated formal operator

$$ik\sqrt{1 + \frac{1}{k_\epsilon^2 R^2} \partial_\theta^2} \quad (8)$$

is then extended as

$$ik\sqrt{1 + \partial_s \left(\frac{1}{k_\epsilon^2} \partial_s \right)} \quad (9)$$

for a general smooth arbitrarily-shaped boundary Σ setting $\epsilon = 0.4k^{1/3}\kappa^{2/3}$. The other corrective terms are kept from the usual classical approach [24] and results in the condition (4). The new regularized and smooth symbol yields a uniform approximation of the DtN operator for any frequency ξ . This is not the case of the usual BGT-like ABC which only models the first propagative modes. Indeed, this condition is a local version of (6) using some second-order Taylor approximants for $k \gg |\xi|$; this remark is completely in accordance with the analytical study developed by Harari and Djellouli in [29]. We must emphasize on the fact that the new ABC is not and cannot be an exact condition. Indeed, the estimate of the almost optimal parameter ϵ is formally developed for a circular cylinder to remove the singularity from the principal symbol. No estimates are available to control the error in the truncation of the approximate pseudodifferential operators and no strong mathematical foundations are yet given for the derivation of this condition. In our opinion, a deeper study would require the development of new pseudodifferential tools to study the behaviour of the DtN map in the transition region. However, these aspects remain a difficult task and further studies are required.

The main drawback of the new boundary condition is that it involves a non-local operator -the square-root operator- which is expensive to compute directly [22]. A possible approach to avoid this drawback consists of using a suitable rational approximation of this operator. This results in the solution to a set of a local differential equations defined on Σ and gives a local representation of this non-local operator which can thus be quickly evaluated. In [22], the approach of Milinazzo *et al.* [23] has been used to propose an efficient approximation of the square-root operator using some complex Padé-type approximations of order N . More precisely, the following approximation (called the rotating branch-cut approximation) is used

$$\sqrt{1+z} \approx C_0 + \sum_{j=1}^N \frac{A_j z}{1+B_j z}, \quad (10)$$

where

$$C_0 = \exp(i\frac{\theta}{2})R_N(\exp(-i\theta) - 1)$$

and

$$A_j = \frac{\exp(-i\frac{\theta}{2})a_j}{(1+b_j(\exp(-i\theta) - 1))^2} \quad B_j = \frac{\exp(-i\theta)b_j}{(1+b_j(\exp(-i\theta) - 1))^2}.$$

Here, θ stands for the chosen angle of rotation and $(a_j, b_j)_{j=1, \dots, N}$ are the standard real Padé coefficients given by

$$a_j = \frac{2}{2N+1} \sin^2\left(\frac{j\pi}{2N+1}\right) \quad b_j = \cos^2\left(\frac{j\pi}{2N+1}\right).$$

We define $R_N(z)$ as the real Padé approximation of the square-root

$$R_N(z) = 1 + \sum_{j=1}^N \frac{a_j z}{1 + b_j z}.$$

Finally, an approximation of order N of the ABC (4) is given by

$$\partial_{\mathbf{n}_\Sigma} u = ik(C_0 u + \sum_{j=1}^N A_j \varphi_j) - \frac{\kappa}{2} u + \frac{\kappa^2}{8(\kappa - ik)} u - \partial_s \left(\frac{\kappa}{2k^2} \partial_s u \right), \quad \text{on } \Sigma, \quad (11)$$

where $\{\varphi_j\}_{j=1, \dots, N}$ are the auxiliary surface functions defined on Σ which fulfill the following differential equations

$$(1 + \partial_s \left(\frac{B_j}{k_\epsilon^2} \partial_s \right)) \varphi_j = \partial_s \left(\frac{1}{k_\epsilon^2} \partial_s \right) u, \quad \text{on } \Sigma, \quad j = 1, \dots, N. \quad (12)$$

Parameters $N = 8$ and $\theta = \pi/4$ have proven to yield the best accuracy in the OSRC techniques. We will again discuss this crucial choice in the sequel in the framework of ABCs.

4. ITERATIVE KRYLOV FINITE ELEMENT SOLUTION

4.1. Variational formulation

To apply the finite element method, the sound-hard scattering problem with the ABC (4)-(10) is written in a variational form: find $(u, \varphi_1, \dots, \varphi_N)$ in $H^1(\Omega) \times H^1(\Sigma)^N$ such that

$$\mathcal{A}(u, v) + \sum_{j=1}^N \mathcal{B}_j(\varphi_j, v) = b(v), \quad \forall v \in H^1(\Omega) \quad (13)$$

where \mathcal{A} is the symmetrical bilinear form defined on $H^1(\Omega) \times H^1(\Omega)$ by

$$\begin{aligned} \mathcal{A}(u, v) = & \int_{\Omega} \nabla u \nabla v d\Omega - k^2 \int_{\Omega} u v d\Omega - ikC_0 \int_{\Sigma} u v d\Sigma + \frac{1}{2} \int_{\Sigma} \kappa u v d\Sigma \\ & - \frac{1}{8} \int_{\Sigma} \frac{\kappa^2}{\kappa - ik} u v d\Sigma + \frac{1}{2k^2} \int_{\Sigma} \kappa \partial_s u \partial_s v d\Sigma. \end{aligned}$$

The spaces $H^1(\Omega)$ and $H^1(\Sigma)$ are the usual Sobolev spaces, respectively on Ω and Σ . For $j = 1, \dots, N$, we have that \mathcal{B}_j is also a symmetrical bilinear form defined on $H^1(\Sigma) \times H^1(\Sigma)$ and given by the following expression

$$\mathcal{B}_j(\varphi_j, v) = -ikA_j \int_{\Sigma} \varphi_j v d\Sigma.$$

The right-hand side b is a linear form related to the initial incident field by the weak representation

$$b(v) = \int_{\Gamma} g v d\Gamma.$$

Obviously, variational equation (13) is not sufficient. It is necessary to add to the system the decoupled differential constraints (12) between the auxiliary functions and the unknown approximate scattered field

$$\mathcal{C}(u, \psi_j) + \mathcal{D}_j(\varphi_j, \psi_j) = 0, \quad \forall \psi_j \in H^1(\Sigma), \quad j = 1, \dots, N, \quad (14)$$

where \mathcal{C} and \mathcal{D}_j are two symmetrical bilinear forms defined on $H^1(\Sigma) \times H^1(\Sigma)$ respectively by

$$\mathcal{C}(u, \psi_j) = \frac{1}{k_\epsilon^2} \int_{\Sigma} \partial_s u \partial_s \psi_j d\Sigma$$

and

$$\mathcal{D}_j(\varphi_j, \psi_j) = \int_{\Sigma} \varphi_j \psi_j d\Sigma - \frac{B_j}{k_\epsilon^2} \int_{\Sigma} \partial_s \varphi_j \partial_s \psi_j d\Sigma.$$

This formulation introduces only some additional mass and stiffness-like matrices linked to the finite element discretization of equations (13) and (14). This particularly interesting aspect of (13) and (14) is related to the fact that the Padé approximation yields a localization of the square-root operator. Moreover, each bilinear form \mathcal{A} , \mathcal{B} , \mathcal{C} and \mathcal{D} is symmetrical. This is an interesting advantage from a memory storage point of view.

At this point of the method, we must emphasize on the fact that other alternative variational formulations could be investigated. This point is important from the practical point of view if one wishes to solve the resulting system by means of an iterative solver. Indeed, the condition number of the system is deeply linked to the variational formulations. Other global symmetrical formulations (and this is not the case here since \mathcal{B} is not the transposed bilinear form of \mathcal{C}) could be investigated. However, it seems that this is at the price of the development of a mixed variational formulation and the use of adapted finite element methods. This aspect can be more specifically observed in the three-dimensional case (because of the presence of the surface divergence and surface gradient operators). But these extensions are beyond the scope of the present paper.

4.2. The Galerkin-Least-Squares finite element method

We will compare two finite element methods in the sequel of the paper. The first one is the classical Galerkin Finite Element Method (FEM). To partially avoid the dispersion effects generally associated to this first technique, we also consider the Galerkin-Least-Squares (GLS) discretization scheme. In the GLS approach, the variational formulation is adjusted to take into account the residual of the partial differential equation. Under this constraint, the stabilized weak form of the equation is

$$\mathcal{A}_{\text{GLS}}(u, v) + \sum_{j=1}^N \mathcal{B}_j(\varphi_j, v) = b, \quad (15)$$

setting $\mathcal{A}_{\text{GLS}}(u, v) = \mathcal{A}(u, v) + \int_{\tilde{\Omega}} \eta \mathcal{L}u \mathcal{L}v d\Omega$, where $\mathcal{L} = (\Delta + k^2)$ is the Helmholtz operator and $\tilde{\Omega}$ designates the union of interior elements. This last choice is generally made according to the regularity requirements of typical, piecewise smooth finite-element functions. One crucial question is the choice of the stabilization parameter η which is generally based on a design criterion. Harari *et al.* [8] evaluate η analytically assuming that the scattered wave is planar. As a result, the accuracy of the obtained results depends on the direction of propagation.

Two values of η corresponding to a direction equal to 0 and to 22.5 degrees are often used in practice [8] for a mesh based on bilinear finite elements. In our numerical experiments, we use the numerical definition of the parameter η proposed by [17]. From numerical investigations, it appears that the η corresponding to 22.5 degrees yields the best results for a mesh based on triangular elements. In the sequel, we only report the numerical results associated to this value. Moreover, this approximation will be compared to the classical linear Galerkin finite element discretization. Numerical results will be reported for comparison.

4.3. Preconditioned iterative Krylov scheme

The linear finite element discretization results in a linear coupled system of equations of the form

$$\begin{pmatrix} \mathbf{A}_h & \mathbf{B}_h \\ \mathbf{C}_h & \mathbf{D}_h \end{pmatrix} \begin{pmatrix} \mathbf{u}_h \\ \boldsymbol{\varphi}_h \end{pmatrix} = \begin{pmatrix} \mathbf{b}_h \\ \mathbf{0}_h \end{pmatrix}, \quad (16)$$

where $\mathbf{u}_h \in \mathbb{C}^{N_h}$ is the unknown complex-valued approximation of the scattered field u and $\boldsymbol{\varphi}_h$ is the complex vector field of discretized auxiliary functions $(\varphi_{1h}, \dots, \varphi_{N_h})$. Hence, this vector is in $\mathbb{C}^{N_{\Sigma_h} N}$, where N_h and N_{Σ_h} are respectively the number of degrees of freedom of the linear finite element method on the interpolated domains Ω_h and Σ_h . Vector $\mathbf{b}_h \in \mathbb{C}^{N_h}$ is given by the linear form b .

The complex linear system (16) is sparse and globally non-symmetric. Furthermore, this is also a non-Hermitian and non-diagonally dominant system of equations. A direct solution can be reached by using a Gauss elimination solver. However, due to the excessive cost of these latter methods, especially at high frequencies for three-dimensional problems where the solution to a large size linear system is required, iterative schemes are generally preferred. This is the reason why we adapt this point of view even if a direct solver could also be used in the two-dimensional case.

The proposed solution is based on the Schur complement which consists of eliminating the unknown $\boldsymbol{\varphi}_h$ in system (16) so that the new system to solve is

$$\mathbf{G}_h \mathbf{u}_h = \mathbf{b}_h \quad \text{setting} \quad \mathbf{G}_h = \mathbf{A}_h - \mathbf{B}_h \mathbf{D}_h^{-1} \mathbf{C}_h. \quad (17)$$

Among the possible iterative methods, a restarted GMRES [20] solver accelerated by an ILUT preconditioner (based on \mathbf{A}_h) is then used [17]. To check that no additional error is introduced in our algorithm, we have fixed the residual of the GMRES to 10^{-6} which (after verifications) is sufficient to have a negligible error compared to the one arising in both the ABC and finite element approximations.

Since our goal is to analyze the accuracy of the new Padé-type ABC, we do not report any result concerning the behavior of the iterative scheme in terms of speed up and convergence rate which are closely linked to the structure of the linear system to be solved (as already mentioned above). However, we must first notice that the added cost linked to the solution to each auxiliary equation is efficiently realized using a restarted GMRES preconditioned by the ILUT technique at a small additional overall cost. Indeed, the convergence is obtained in 2 or 3 iterations with an excellent accuracy. A second point is that the convergence breakdown of the iterative scheme observed in [17] can be overcome by adding a damping parameter to the Helmholtz operator with which the preconditioner is built. Finally, to obtain a more efficient preconditioner for the iterative solution, we should rather consider the matrix \mathbf{G}_h for building a suitable preconditioner, as in the case of generalized saddle point problems [36]. This very

difficult aspect for highly indefinite linear systems is beyond the scope of this paper and further investigations are still required.

Concerning the memory storage, the additional cost compared to the one associated to the BGT-like ABC is only linked to the surface linear systems resulting from the auxiliary equations. We will later see that $N = 2$ equations is sufficient for a very important reduction of the volumetric mesh. So globally, for one given problem using a close fictitious boundary Σ , the memory will be slightly increases but with a gain of accuracy. For comparison, we will report the global memory storage for each solution in terms of number of coefficients of our matrix representations during the numerical experiments.

5. PERFORMANCES AND COMPARISONS FOR SOME MODEL TEST PROBLEMS

We consider in this section two model sound-hard scatterers to test the proposed algorithm: a unit circular cylinder \mathcal{D} and an elliptical cylinder \mathcal{E} with a major semi-axis equal to $a = 1$ and a minor semi-axis equal to $b = 0.2$, both centered at the origin. The reference solution is computed by using the CHIEF integral equation method developed in [37]. The mesh resolution for this technique has been fixed to 80 elements per wavelength.

5.1. The sound-hard circular cylinder

In all the computations, we assume that \mathcal{D} is illuminated by a plane wave with a zero-degree incidence. The wave number is set to $k = 50$. The circular fictitious boundary is placed at a distance $m\lambda$ from the scatterer. The average mesh resolution -the average number of elements per wavelength- is given by $n_\lambda = \lambda/h_{\max}$, where h_{\max} is the largest element size of the finite element method. The relative Root-Mean Square (RMS) error (in percents) on the computational domain Ω_h (respectively Γ_h) is computed in the $L_2(\Omega_h)$ -norm (respectively $L_2(\Gamma_h)$ -norm) with respect to the reference analytical solution expressed as a Mie series. We also compute the far-field pattern given by the scattering amplitude

$$a_\infty(\vartheta) = \frac{e^{-i\frac{\pi}{4}}}{\sqrt{8\pi k}} \int_{\Gamma} (\partial_{\mathbf{n}_\Gamma(y)} u(y) - ik\boldsymbol{\vartheta} \cdot \mathbf{n}_\Gamma(y)u(y)) e^{-ik\boldsymbol{\vartheta} \cdot \mathbf{y}} d\Gamma(y) \quad (18)$$

through the bistatic Radar Cross Section (RCS) (also called the target strength)

$$\text{RCS}(\vartheta) = 10 \log_{10}(2\pi |a_\infty(\vartheta)|^2) \quad (\text{dB}),$$

setting $\boldsymbol{\vartheta} = (\cos(\vartheta), \sin(\vartheta))^T$.

Let us begin by setting the two parameters N and θ defining the Padé-type ABC. We present in Tables I (for $m = 0.25$) and II (for $m = 1$) the error in the computational domain and on the trace by increasing the number of auxiliary Padé functions and modifying the rotation angle θ between 0 and $\pi/2$. The resolution of the Galerkin FEM is $n_\lambda = 40$ to obtain a satisfactory accuracy. A judicious choice of angle is $\theta = \pi/6$ or $\theta = \pi/3$ and $N = 2$. In the sequel, we report the results for these two angles. Generally speaking, $\pi/6$ yields a better accuracy than $\pi/3$ for a closer boundary. This will be essential in the case of the submarine-shaped scatterer. However, to notice the sensitivity of the results according to θ and for the sake of completeness, we choose to also report the results concerning $\pi/3$. We do not give here the results for $N = 1$ which yield a similar accuracy as for the BGT-like ABC.

Table I. RMS relative error on the interior solution (on the trace) of the computed scattered field for different values of the parameters defining the Padé-type ABC and the BGT-like ABC. The mesh resolution is fixed to $n_\lambda = 40$ and $m = 0.25$ for the Galerkin scheme.

	$N = 2$	$N = 4$	$N = 8$	BGT
$\theta = 0$	3.30 (3.08)	5.57 (5.26)	4.63 (4.41)	17.40 (17.18)
$\theta = \pi/6$	1.94 (1.91)	4.35 (4.12)	4.68 (4.45)	17.40 (17.18)
$\theta = \pi/3$	4.07 (3.95)	4.64 (4.12)	4.67 (4.44)	17.40 (17.18)
$\theta = \pi/2$	6.02 (6.18)	4.81 (4.58)	4.67 (4.44)	17.40 (17.18)

Table II. RMS relative error on the interior solution (on the trace) of the computed scattered field for different values of the parameters defining the Padé-type ABC and the BGT-like ABC. The mesh resolution is fixed to $n_\lambda = 40$ and $m = 1$ for the Galerkin scheme.

	$N = 2$	$N = 4$	$N = 8$	BGT
$\theta = 0$	1.16 (0.73)	1.08 (0.76)	1.08 (0.76)	8.04 (8.80)
$\theta = \pi/6$	1.22 (0.87)	1.08 (0.76)	1.08 (0.76)	8.04 (8.80)
$\theta = \pi/3$	1.26 (1.07)	1.08 (0.76)	1.08 (0.76)	8.04 (8.80)
$\theta = \pi/2$	3.35 (4.21)	1.06 (0.71)	1.08 (0.76)	8.04 (8.80)

Table III. Circular cylinder: RMS error for different mesh resolutions of the Galerkin FEM and ABC positions. The values in parenthesis correspond to the error on the trace.

m	n_λ	N_h	N_{Σ_h}	BGT	Padé ($\pi/6, 2$)	Padé ($\pi/3, 2$)
0.125	10	998	499	21.31(21.31)	8.03(7.32)	10.70(10.23)
	20	2997	999	21.66(21.45)	2.64(2.40)	5.79(5.66)
	40	9995	1999	21.76(21.48)	1.97(1.90)	4.71(4.64)
0.25	10	1497	499	18.15(17.81)	8.99(7.78)	11.24(10.28)
	20	5994	999	17.45(17.25)	3.00(2.75)	5.40(5.17)
	40	21989	1999	17.40(17.18)	1.94(1.91)	4.07(3.95)
0.5	10	2994	499	16.38(15.15)	10.70(7.76)	11.74(8.78)
	20	10989	999	13.03(13.37)	3.48(2.81)	4.47(3.69)
	40	41979	1999	12.39(12.97)	1.81(1.76)	2.90(2.70)
1	10	4990	499	19.17(11.50)	16.11(7.64)	15.91(7.53)
	20	19980	999	9.51(8.61)	4.14(1.86)	4.00(2.01)
	40	79960	1999	8.04(8.80)	1.22(0.87)	1.26(1.07)
2	10	9980	499	26.99(8.84)	26.37(7.55)	26.35(7.61)
	20	39960	999	7.97(4.16)	6.99(2.02)	7.03(2.16)
	40	159920	1999	3.75(4.06)	1.76(0.64)	1.78(0.64)

Let us now investigate in details the accuracy issue linked to the new ABC. To that end, we report on Tables III (Galerkin) and IV (GLS) the error on both the computational domain and the trace accordingly to the size of the computational domain at different mesh resolutions. For each case, the mesh is described by N_h and N_{Σ_h} . We clearly see that for an *a priori* fixed error, we can move the fictitious boundary closer to the scatterer for the Padé-type ABC without a significant deterioration in accuracy. This is not the case of the usual BGT-like ABC which can yield a poor precision. This remark shows that we can significantly reduce the size of the computational domain using the new ABC. Moreover, for a distance $m\lambda$ and a given mesh

Table IV. Circular cylinder: RMS error for different mesh resolutions of the GLS_{22.5} FEM and ABC positions. The values in parentheses correspond to the error on the trace.

m	n_λ	N_h	N_{Σ_h}	BGT	Padé ($\pi/6, 2$)	Padé ($\pi/3, 2$)
0.125	10	998	499	21.73(21.81)	7.23(7.26)	9.65(9.75)
	20	2997	999	21.71(21.49)	2.08(1.98)	5.31(5.25)
	40	9995	1999	21.76(21.48)	1.81(1.76)	4.57(4.50)
0.25	10	1497	499	17.94(17.98)	8.39(9.19)	10.18(10.88)
	20	5994	999	17.27(17.02)	2.32(2.37)	4.82(4.75)
	40	21989	1999	17.34(17.11)	1.70(1.70)	3.88(3.78)
0.5	10	2994	499	13.29(12.14)	8.48(7.75)	9.62(8.80)
	20	10989	999	12.10(12.27)	2.90(2.37)	3.75(3.47)
	40	41979	1999	12.16(12.68)	1.49(1.56)	2.73(2.62)
1	10	4990	499	12.59(7.35)	12.10(8.38)	12.33(8.85)
	20	19980	999	7.67(7.59)	3.15(2.27)	3.39(2.74)
	40	79960	1999	7.66(8.59)	1.14(1.09)	1.41(1.40)
2	10	9980	499	19.52(6.20)	19.68(8.08)	19.70(8.17)
	20	39960	999	5.65(3.10)	5.14(2.22)	5.17(2.23)
	40	159920	1999	3.30(3.87)	1.34(0.80)	1.37(0.67)

Table V. Circular cylinder: RMS error for different mesh resolutions of the GLS FEM and BGT-like ABC positions. The values in parentheses correspond to the error on the trace.

m	n_λ	GLS_0	$GLS_{22.5}$	GLS_{30}	GLS_{45}	GLS_{60}	GLS_{90}
0.125	10	22.40(22.48)	21.73(21.81)	21.91(21.99)	23.33(23.31)	23.33(23.31)	22.45(22.53)
	20	21.79(21.55)	21.71(21.49)	21.74(21.51)	21.85(21.60)	21.98(21.72)	21.80(21.56)
	40	21.78(21.49)	21.76(21.48)	21.77(21.49)	21.79(21.50)	21.82(21.53)	21.78(21.49)
0.25	10	19.13(19.21)	17.94(17.98)	18.21(18.22)	19.52(19.48)	19.97(19.76)	19.21(19.28)
	20	17.21(16.87)	17.27(17.02)	17.26(16.99)	17.21(16.87)	17.22(16.84)	17.21(16.87)
	40	17.31(17.05)	17.34(17.11)	17.33(17.10)	17.31(17.06)	17.31(17.04)	17.31(17.05)
0.5	10	13.35(12.24)	13.28(12.14)	13.25(12.02)	13.57(12.21)	12.97(11.40)	13.35(12.24)
	20	11.44(11.38)	12.10(12.28)	12.00(12.15)	11.50(11.44)	10.99(10.78)	11.41(11.34)
	40	11.94(12.40)	12.16(12.68)	12.13(12.64)	11.96(12.42)	11.82(12.24)	11.93(12.39)
1	10	13.28(9.98)	12.59(7.35)	13.16(7.80)	14.70(10.16)	14.39(11.29)	13.38(10.10)
	20	7.02(7.45)	7.67(7.59)	7.63(7.57)	7.25(7.52)	6.80(7.60)	7.00(7.46)
	40	7.43(8.50)	7.66(8.59)	7.63(8.58)	7.46(8.52)	7.36(8.54)	7.42(8.50)
2	10	19.00(9.40)	19.52(6.10)	20.51(6.55)	21.48(9.22)	19.66(10.77)	19.05(9.53)
	20	5.29(3.36)	5.65(3.10)	5.87(3.11)	6.03(3.37)	5.42(3.62)	5.30(3.39)
	40	3.15(3.81)	3.30(3.87)	3.31(3.86)	3.25(3.83)	3.13(3.82)	3.15(3.81)

resolution n_λ , the Padé-type ABC leads to a much smaller error than the BGT-like ABC. Once again, we do not report here the error associated to the case $N = 1$ which is similar to the one obtained with the BGT-like condition. According to the previous results, we can then get a smaller domain of computation or an improvement in accuracy during the simulation if we use the Padé-type ABC. This conclusion can be related to the property that, unlike the BGT-like ABC, the new ABC is built to include both the propagative and the evanescent harmonics involved in the scattered field. Moreover, the latter condition incorporates in an approximate way the high order harmonics present in the field computation and which can propagate near a tangential direction to the fictitious boundary; the harmonics are more important when Σ is close to Γ . We also notice that a mesh resolution $n_\lambda = 20$ mostly leads to an acceptable

Table VI. Circular cylinder: RMS error for different mesh resolutions of the GLS FEM and Padé($\pi/6, 2$) ABC positions. The values in parentheses correspond to the error on the trace.

m	n_λ	GLS_0	$GLS_{22.5}$	GLS_{30}	GLS_{45}	GLS_{60}	GLS_{90}
0.125	10	8.12(8.58)	7.23(7.27)	7.37(7.50)	8.24(8.72)	7.80(8.34)	8.17(8.64)
	20	1.96(1.96)	2.08(1.98)	2.02(1.95)	1.87(1.89)	1.54(1.57)	1.96(1.97)
	40	1.72(1.67)	1.81(1.76)	1.79(1.73)	1.68(1.63)	1.62(1.57)	1.71(1.67)
0.25	10	12.00(13.47)	8.39(9.19)	9.29(10.20)	12.97(14.28)	13.80(15.32)	12.19(13.65)
	20	2.31(2.60)	2.32(2.37)	2.31(2.38)	2.36(2.60)	2.05(2.37)	2.31(2.60)
	40	1.53(1.55)	1.71(1.70)	1.68(1.67)	1.54(1.55)	1.41(1.43)	1.52(1.54)
0.5	10	12.46(13.50)	8.48(7.75)	9.15(8.56)	12.80(13.17)	14.83(15.94)	12.65(13.71)
	20	3.16(3.57)	2.50(2.37)	2.59(2.51)	3.27(3.51)	3.51(3.96)	3.20(3.61)
	40	1.39(1.57)	1.49(1.56)	1.48(1.55)	1.42(1.57)	1.35(1.56)	1.39(1.57)
1	10	14.58(11.87)	12.10(8.38)	13.01(8.97)	13.01(8.97)	15.92(11.91)	14.75(12.01)
	20	3.84(3.31)	3.15(2.27)	3.38(2.43)	4.18(3.27)	4.26(3.63)	3.88(3.35)
	40	1.26(1.30)	1.14(1.09)	1.18(1.12)	1.33(1.29)	1.33(1.39)	1.27(1.31)
2	10	19.54(11.15)	19.68(8.08)	20.70(8.41)	21.86(10.97)	20.17(12.17)	19.60(11.27)
	20	5.14(3.13)	5.14(2.23)	5.42(2.32)	5.84(3.05)	5.38(3.47)	5.16(3.17)
	40	1.36(1.01)	1.34(0.80)	1.41(0.82)	1.53(0.99)	1.42(1.09)	1.36(1.02)

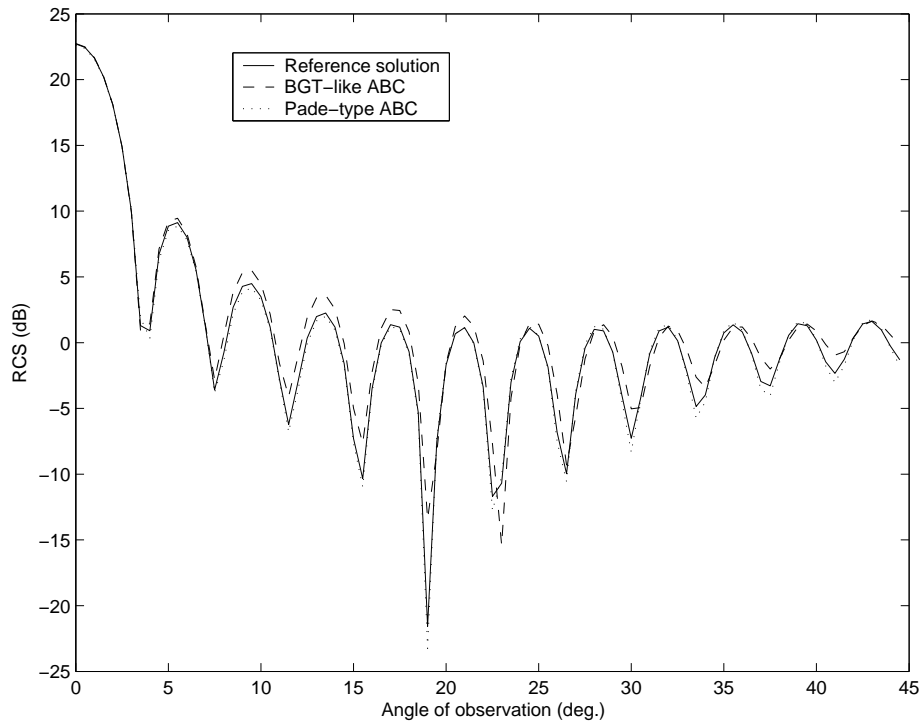
Table VII. Circular cylinder: RMS error for different mesh resolutions of the GLS FEM and Padé($\pi/3, 2$) ABC positions. The values in parentheses correspond to the error on the trace.

m	n_λ	GLS_0	$GLS_{22.5}$	GLS_{30}	GLS_{45}	GLS_{60}	GLS_{90}
0.125	10	9.62(10.08)	9.65(9.75)	9.56(9.74)	9.40(9.90)	8.38(8.98)	9.62(10.08)
	20	5.01(4.99)	5.31(5.25)	5.21(5.16)	4.84(4.83)	4.84(4.83)	4.99(4.98)
	40	4.46(4.40)	4.57(4.50)	4.54(4.47)	4.41(4.35)	4.32(4.26)	4.46(4.40)
0.25	10	12.38(13.83)	10.18(10.88)	11.64(11.48)	12.94(14.32)	13.09(14.76)	12.50(13.96)
	20	4.50(4.60)	4.82(4.75)	4.77(4.73)	4.54(4.62)	4.12(4.27)	4.48(4.59)
	40	3.72(3.64)	3.88(3.78)	3.86(3.77)	3.73(3.65)	3.61(3.54)	3.71(3.64)
0.5	10	12.83(13.87)	9.62(8.80)	10.15(9.47)	13.19(13.58)	14.94(16.19)	12.99(14.07)
	20	4.09(4.37)	3.75(3.47)	3.80(3.57)	4.19(4.32)	4.30(4.72)	4.12(4.41)
	40	2.64(2.64)	2.73(2.62)	2.72(2.62)	2.66(2.64)	2.60(2.05)	2.64(2.64)
1	10	14.95(12.42)	12.33(8.85)	13.27(9.46)	13.26(9.46)	17.01(13.99)	15.12(12.57)
	20	4.21(3.80)	3.39(2.74)	3.63(2.90)	4.52(3.75)	4.67(4.15)	4.25(3.84)
	40	1.62(1.60)	1.41(1.40)	1.46(1.44)	1.67(1.64)	1.72(1.75)	1.63(1.66)
2	10	19.58(11.14)	19.70(8.17)	20.73(8.48)	21.86(11.00)	20.17(12.09)	19.62(11.25)
	20	5.15(3.08)	5.17(2.23)	5.44(2.31)	5.84(2.99)	5.38(3.40)	5.16(3.11)
	40	1.33(0.87)	1.34(0.67)	1.40(0.69)	1.50(0.85)	1.39(0.95)	1.36(0.88)

accuracy, in particular in the calculation of the trace. This can be further slightly reduced with the help of the GLS scheme. The reduction in the size of the computational domain partially limits the pollution effects which are generally involved in a FEM at high-frequencies (see [10] for a similar remark in the case of the BGT-like ABC). These two aspects are crucial since they allow an accurate computation of the scattered field based on the Helmholtz integral representation (18).

To analyze how the effect of the angle is involved in the GLS scheme, we report on Tables V, VI and VII, the errors of the GLS scheme for different angles and ABCs. A first observation is that, in the case of the BGT-like ABC, the error is not always decaying according to the mesh size. This can be explained by the fact that we compute the error between the exact Mie

Figure 1. Far-field pattern (between 0 and 45 degrees) of the unit circular cylinder using the BGT-like ABC.



series solution and the BGT solution. Since there is always an important analytical error if the fictitious boundary is placed close enough to the scatterer, the convergence of the finite element method is polluted by this analytical error. However, this latter error tends to disappear as m grows and the convergence of the finite element solution is again observed more clearly. We do not observe this problem with the Padé-type ABC which exhibits a much higher accuracy. Let us now consider Table VI. We remark that, from a general point of view, the direction 22.5 degrees is not far from being optimal to design a reliable GLS scheme for some densities $n_\lambda = 10$ and $n_\lambda = 20$. This is in accordance with the results derived by Harari and Nogueira in [38]. As a consequence, from now on, we will consider this almost optimal direction in the GLS scheme.

To end this section, we display in Figure 1 a part of the RCS associated to the BGT-like and Padé-type ABCs (setting $\theta = \pi/6$). The parameters are set to $k = 50$, $m = 0.125$ and the mesh resolution is $n_\lambda = 20$ points per wavelength for the GLS method. We immediately observe that the computed RCS for the Padé-type condition is much more accurate than using the BGT-like condition. A similar accuracy for this latter condition would have required the placement of the boundary at $m = 2$ wavelengths. Thus, this would have dramatically increased the size

Table VIII. Elliptical cylinder: RMS error on the trace for different mesh resolutions of the GLS_{22.5} FEM and ABC positions (on a circular (C) or elliptical shaped fictitious boundary). The values between parentheses correspond to the Galerkin FEM.

m	n_λ	N_h	N_{Σ_h}	BGT	Padé ($\pi/6, 2$)	Padé ($\pi/3, 2$)
0.125(C)	10	19325	508	6.85(11.32)	6.75(11.31)	6.75(11.33)
	20	76480	1016	1.85(2.98)	1.45(2.88)	1.45(2.89)
	40	304378	2031	1.31(1.31)	0.35(0.76)	0.35(0.77)
0.125	10	678	342	37.93(37.90)	6.65(10.58)	12.85(18.18)
	20	2183	684	38.46(38.38)	8.45(9.29)	10.92(12.24)
	40	7778	1366	38.70(38.72)	9.98(10.12)	11.05(11.34)
0.25	10	1104	348	33.21(35.68)	9.22(12.68)	14.44(19.09)
	20	3923	698	35.17(35.92)	6.49(8.32)	9.37(11.41)
	40	15021	1396	35.88(35.04)	7.95(8.37)	9.56(10.04)
0.5	10	2023	362	24.20(36.74)	14.83(12.90)	17.79(16.35)
	20	7724	724	32.09(35.17)	4.60(7.34)	9.32(9.32)
	40	29735	1448	33.14(34.71)	5.45(6.25)	7.15(7.68)
1	10	4078	391	19.04(30.07)	10.61(10.22)	12.82(9.75)
	20	15591	782	23.14(25.63)	3.64(3.70)	5.30(3.81)
	40	61599	1564	24.45(25.03)	3.16(3.13)	4.06(3.59)
1.5	10	6239	420	13.75(13.43)	9.55(12.23)	10.47(12.96)
	20	24335	840	15.60(14.99)	2.27(3.42)	3.14(4.07)
	40	96223	1680	16.38(16.22)	1.88(2.09)	2.26(2.44)
2	10	8566	449	9.17(17.29)	7.88(11.59)	8.34(11.47)
	20	33645	899	10.16(11.91)	2.30(2.95)	2.69(2.88)
	40	146847	1883	10.92(11.31)	1.34(1.41)	1.45(1.32)

of the finite element mesh and the associated linear system to solve. Finally, all the results presented here extend to higher wave numbers. Moreover, a better accuracy is still observed when solving the sound-soft scattering problem.

5.2. The sound-hard elliptical cylinder

We now consider the sound-hard elliptical scatterer \mathcal{E} illuminated by a plane wave at a frequency $k = 50$ for an incidence angle equal to $\theta^{\text{inc}} = 20$ degrees. We report in Table VIII the RMS error on the trace of the computed solution for various ABCs for both the Galerkin (in parentheses) and GLS schemes. We first choose a circular (C) fictitious boundary placed at a distance $R = a + m\lambda$ from the scatterer taking $m = 0.125$. As we can observe, we get a good agreement between the solutions. However, due to the mismatch between the shape of a circular fictitious boundary and an elliptical scatterer, the number of degrees of freedom required in the solution procedure remains large. The mesh size cannot be further reduced. To circumvent this problem, we rather choose an elliptical-shaped fictitious boundary Σ taken conformal to the scatterer by setting its two semi-axes a' and b' to $a' = a + m\lambda$ and $b' = b + m\lambda$. We give the results in Table VIII. We can first notice that an important error arises if the BGT-like ABC is used. We also observe some fluctuations in the convergence of the solution even if we refine the mesh. Once again, and like the circular cylinder case, this can be associated to the convergence process between the integral equation and ABC solutions. If we now consider the Padé-type condition, we obtain a noticeable reduction in the error on the trace compared to the one obtained using the BGT-like ABC. Moreover, the GLS solution yields an interesting improvement over the usual Galerkin procedure. If we consider for example $m = 1$ for the

Table IX. Elliptical cylinder: RMS error on the trace for different mesh resolutions of the GLS_{22.5} FEM and ABC positions on a rectangular-shaped fictitious boundary. The values between parentheses correspond to the Galerkin FEM.

m	n_λ	N_h	N_{Σ_h}	BGT	Padé ($\pi/6, 2$)	Padé ($\pi/3, 2$)
0.125	10	2054	390	37.44(39.80)	11.58(9.03)	11.56(14.65)
	20	7744	780	39.13(39.86)	8.83(9.38)	7.99(9.57)
	40	30120	1560	39.81(39.99)	10.42(10.56)	9.05(9.38)
0.25	10	2622	396	33.33(38.99)	10.64(10.70)	12.54(14.78)
	20	9858	791	36.75(38.14)	6.76(8.04)	6.97(8.62)
	40	38401	1584	37.72(38.06)	7.82(8.14)	6.96(7.42)
0.5	10	3838	417	25.37(38.36)	10.79(10.90)	12.90(12.25)
	20	14726	837	31.26(34.74)	4.77(6.38)	6.56(7.17)
	40	57631	1674	33.13(33.96)	5.02(5.59)	5.38(5.71)
1	10	6303	454	16.25(22.27)	8.63(12.06)	9.92(11.69)
	20	24786	906	17.74(18.56)	3.69(4.30)	5.20(4.98)
	40	98160	1820	18.69(18.49)	3.74(3.83)	4.83(4.72)
2	10	8566	449	7.15(14.94)	8.58(11.34)	9.10(11.41)
	20	33645	899	6.71(8.54)	4.51(5.19)	5.47(5.94)
	40	146847	1883	7.23(7.64)	4.45(4.37)	5.26(5.30)

elliptical shape, then we get an error of 3.64% on the trace for $n_\lambda = 20$ (GLS procedure) and obtain a correct bistatic RCS computation for the Padé-type ABC (for $\theta = \pi/6$) as shown on Figures 3 and 2. An error of a few decibels is observable when the BGT-like ABC is used showing its limited accuracy in this configuration.

We now consider the possibility of reducing the size of the computational domain utilizing a rectangular-shaped fictitious boundary. To that end, we consider the rectangle Σ defined by the half-lengths along the x and y directions: $L = a + m\lambda$ and $\ell = b + m\lambda$. We report on Table IX the results obtained for different mesh sizes. We can observe the better behavior of the Padé-type ABC over the BGT-like ABC even if the artificial boundary has some corners. This choice of shape shows that significant savings can be obtained with respect to the mesh size. For instance, we get an error of 4.77% on the trace for $m = 0.5$ and a density $n_\lambda = 20$ for the Padé condition. This results in a nontrivial reduction of the computational domain. A similar accuracy can be obtained with the BGT radiation condition but for a much larger computational domain. In the same situation, we get an error of about 31%.

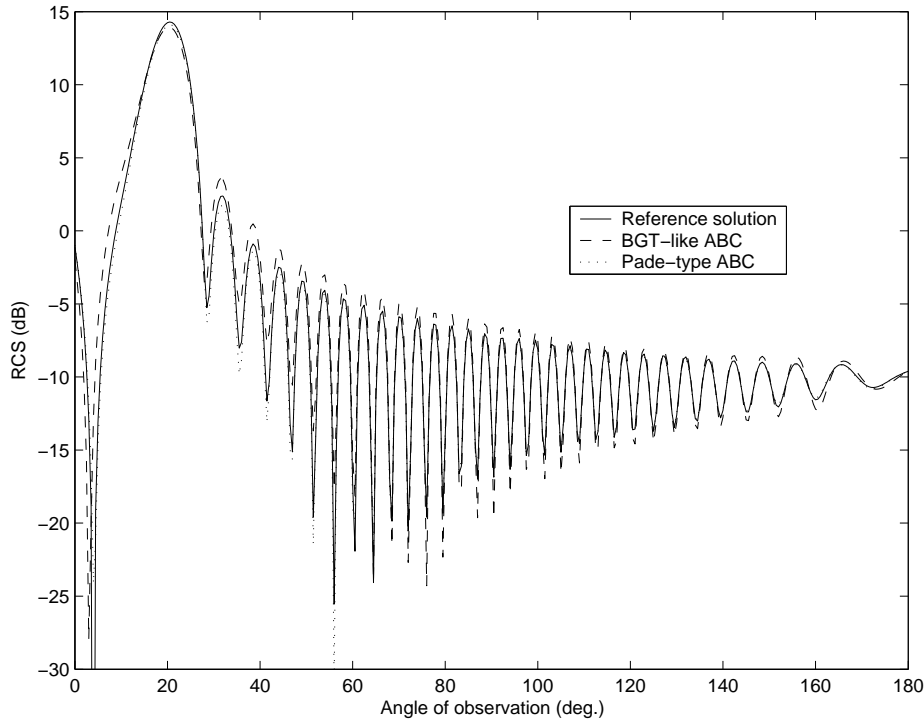
From these first experiments, we conclude that the new Padé-type ABC can lead to a gain both in accuracy and memory savings by reducing the size of the computational domain compared to the usual BGT-like ABC. Moreover, the shape of the fictitious boundary can be optimized without loss of accuracy and efficiency. This adaptive capacity of this ABC to flexible general (convex) shapes allows us to solve more realistic scattering problems such as the one proposed in the section below: the scattering problem by a submarine-shaped scatterer.

6. SOUND-HARD SUBMARINE-SHAPED SCATTERER

Let us now consider a more complex target: the submarine-shaped scatterer plotted in Figure 4. For the computations, we set the parameters to $L = 11$, $D = 1$ and $l = 0.5$.

To show that the above efficiency and accuracy are also realized in the far-field zone, we

Figure 2. Far-field pattern (between 0 and 180 degrees) of the elliptical cylinder using the BGT-like and Padé-type ABCs.

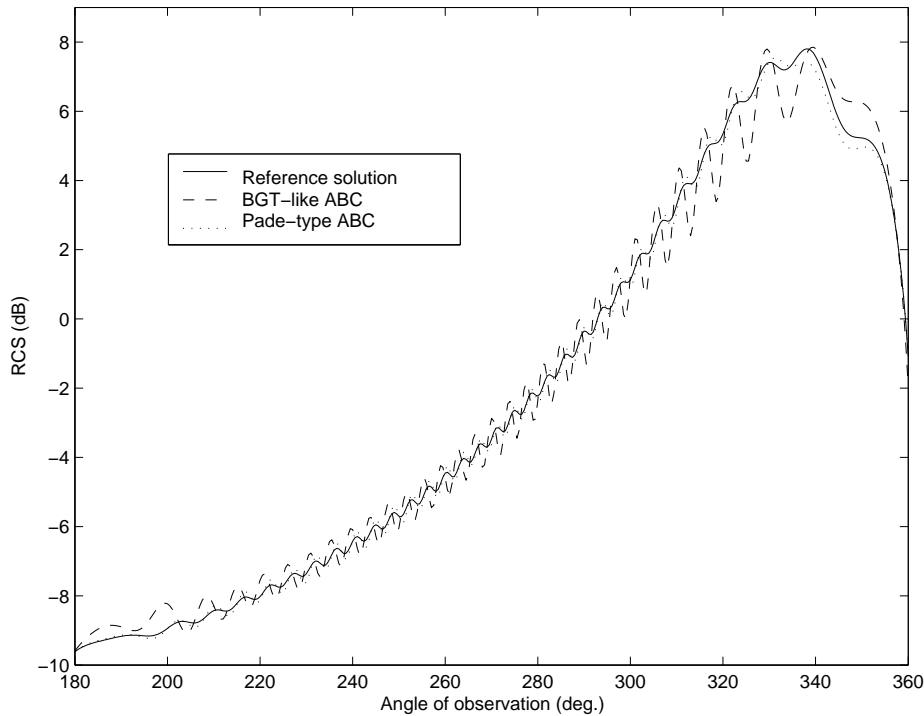


plot the RCS of the submarine-shaped scatterer for the reference solution in Figures 5 and 6. We compare the computations for the BGT-like and Padé-type ABCs set at $m = 0.5$ for a density of $n_\lambda = 20$ points per wavelength. We observe that the complicated structure of the far-field pattern is well-reproduced using the Padé-type condition while errors are visible for the BGT-like ABC.

The direction of the incident wave is set to $\theta^{\text{inc}} = 225$ degrees and the wave number k is chosen as $kD = 15$. This incident wave is known for producing the higher error in the field computation [10]. A first calculation is reported for a circular (C) fictitious boundary, different ABCs and two positions m . Even if a good agreement is reached, this does not significantly reduce the size of the linear system to be solved, and there is finally no significant gain in terms of mesh size. Once again, the main drawback of the circular boundary is that it is not suitable for an elongated body such as that of the submarine-shaped scatterer.

We now specify the two ABCs on an elliptical boundary Σ having the following parameters $(a', b') = (L/2 + m\lambda, D/2 + l + m\lambda)$. We report the results for the two angles $\theta = \pi/6$ and $\theta = \pi/3$. We see that the BGT-like ABC yields a correct accuracy but requires an important computational domain. Concerning the Padé-type ABC, a very impressive gain arises for the

Figure 3. Far-field pattern (between 180 and 360 degrees) of the elliptical cylinder using the BGT-like and Padé-type ABCs.



angle $\theta = \pi/6$ which allows the consideration of much smaller domains for a good accuracy. A good precision is also obtained for the angle $\theta = \pi/3$. This shows again that $\theta = \pi/6$ seems to be a kind of "optimal angle" for the new ABC if small domains are to be considered. This impressive decrease in the size of Ω_h leads to a powerful tool for prospecting high frequency scattering problems for complicated scatterers.

For completeness, we give in Table XI the error on the trace if the submarine-shaped scatterer is surrounded by the rectangular fictitious boundary centered at the origin and defined by the two lengths $a = L + 2m\lambda$ and $b = D + l + 2m\lambda$ along the x and y -axes respectively (the boundary is placed at a distance $m\lambda$ from the extremities of the submarine-shaped scatterer). Once again, we observe a better accuracy of the Padé-type ABC over the BGT-like ABC and the possibility of reducing the size of the computational domain. Unlike the elliptical-shaped fictitious surface, we do not observe a noticeable difference in the accuracy of the computed solutions according to the angle θ . Moreover, the use of the smoother elliptical fictitious boundary leads to a better approximation of the scattered field for a given number of discretization points. This should be related to the fact that the rectangular boundary has some corners which can partially reflect back the wave striking Σ . Corner compatibility conditions are therefore required (cf.

Figure 4. The submarine-shaped scatterer.

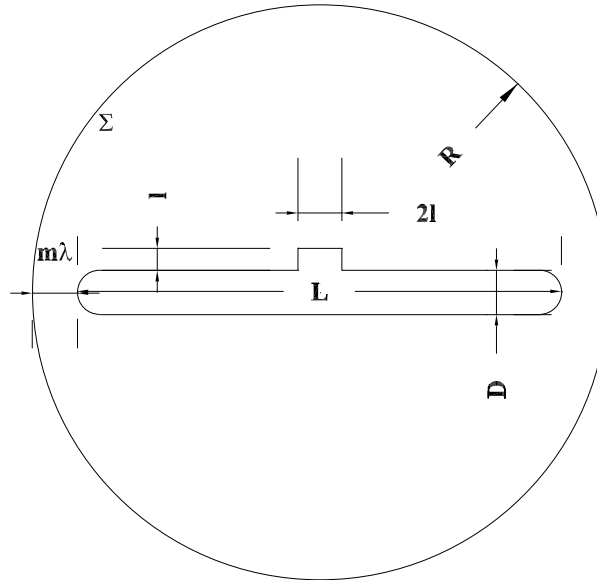
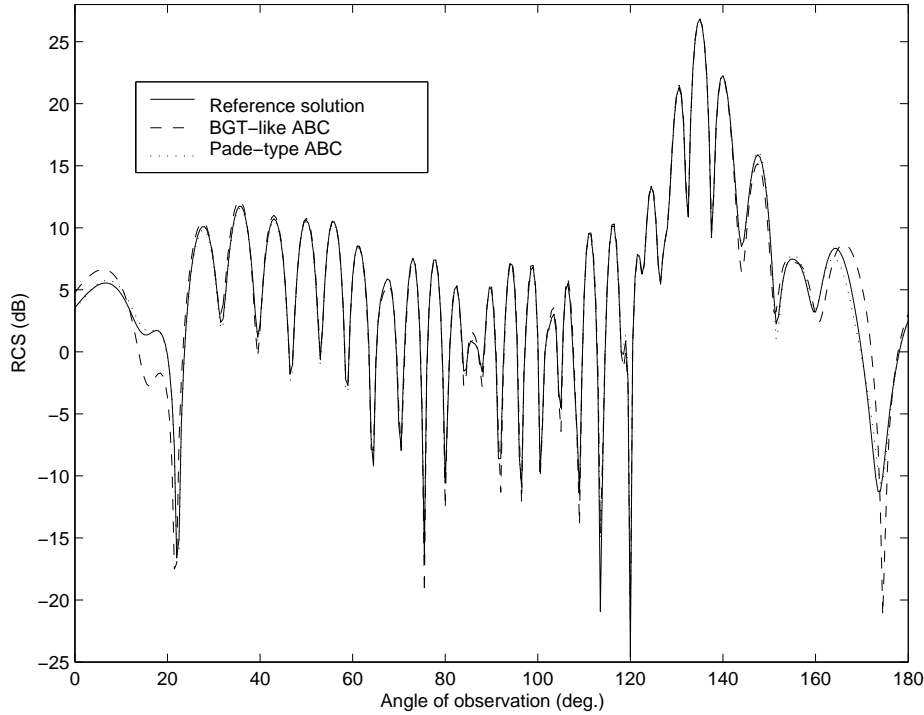


Table X. Submarine shaped scatterer: RMS error on the trace for different mesh resolutions of the GLS_{22.5} FEM and ABC positions on a circular (C) or elliptical shaped fictitious boundary. The values in parentheses correspond to the Galerkin FEM.

m	n_λ	N_h	N_{Σ_h}	BGT	Padé $(\pi/6, 2)$	Padé $(\pi/3, 2)$
0.125(C)	10	56429	833	6.15(14.08)	5.69(14.02)	5.68(14.02)
	20	224151	1666	2.54(4.22)	1.33(3.67)	1.31(3.66)
	40	896663	3331	2.25(2.40)	0.54(1.01)	0.51(1.00)
1(C)	10	65153	888	5.42(14.23)	5.46(14.23)	5.46(14.22)
	20	224151	1776	1.48(3.74)	1.40(3.66)	1.40(3.67)
	40	1034390	3551	0.74(1.18)	0.48(0.98)	0.47(0.99)
0.5	10	7225	572	15.77(24.58)	8.74(15.01)	10.89(16.42)
	20	27990	1152	18.83(21.27)	3.87(6.37)	5.33(7.26)
	40	110182	2302	19.73(20.34)	3.83(4.50)	4.74(5.26)
1	10	10254	606	12.87(23.75)	7.48(15.40)	8.89(15.53)
	20	40293	1204	14.34(16.42)	2.81(4.87)	3.93(4.95)
	40	159432	2414	15.04(15.46)	2.64(2.99)	3.40(3.42)
2	10	16937	660	9.30(15.65)	7.53(13.67)	8.24(13.74)
	20	66900	1321	10.67(11.24)	2.30(3.84)	2.92(4.16)
	40	265586	2642	11.33(11.39)	1.65(1.80)	2.03(2.15)
4	10	32422	778	7.37(15.34)	7.29(13.78)	7.58(13.83)
	20	128900	1556	5.82(7.53)	1.67(3.64)	1.94(3.68)
	40	514549	3111	6.29(6.55)	0.84(1.15)	0.92(1.15)

Figure 5. Far-field pattern (between 0 and 180 degrees) of the submarine-shaped scatterer using the BGT-like and Padé-type ABCs.

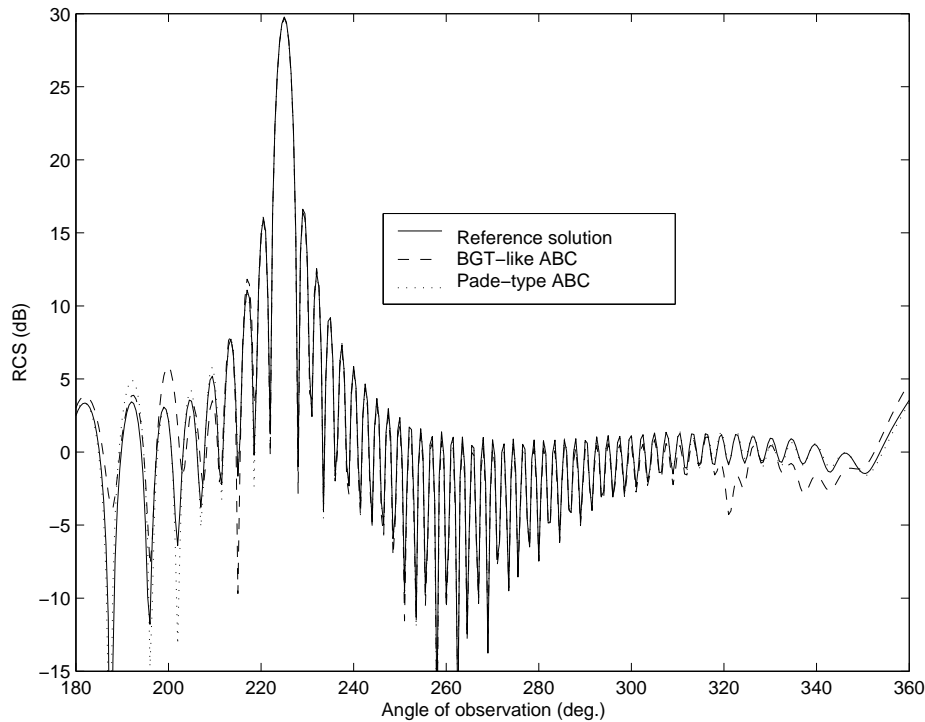


for instance [39] for the wave equation).

7. CONCLUSION

In this paper, we have proposed a numerical study of a new non-reflecting boundary condition for solving two-dimensional acoustic scattering problems in the high-frequency regime. This Padé-type ABC can be applied on any convex fictitious boundary, and allows us to deal with scattering problems involving elongated scatterers (such as a submarine-shaped scatterer, for instance) on some optimized fictitious shapes. Moreover, for high-frequencies, this ABC exhibits a much higher accuracy over the usual BGT-like ABC for relatively small computational domains. Finally, this condition can be easily implemented in a GLS finite element iterative solver to improve the global accuracy of the solution. The natural extension of the ABC to three-dimensional acoustic scattering follows the ideas presented here, and will be the subject of further works. A similar ABC has been derived in [40] for the three-dimensional Maxwell's equations and should lead to a similar behavior. Its numerical approximation is

Figure 6. Far-field pattern (between 180 and 360 degrees) of the submarine-shaped scatterer using the BGT-like and Padé-type ABCs.



under progress. Finally, the improvement of the efficient iterative solution to the resulting linear system using the new ABC is still being studied. Its particular form requires the use of adapted preconditioners to accelerate the convergence rate of the GMRES solver. However, other kinds of efficient solver could also be proposed, and adapted to the results presented here.

ACKNOWLEDGEMENTS

The authors are grateful to the referees for their fruitful comments which have helped us to improve both the form and content of the paper.

Table XI. Submarine shaped scatterer: RMS error on the trace for different mesh resolutions of the GLS_{22.5} FEM and ABC positions on the rectangular fictitious boundary. The values in parentheses correspond to Galerkin FEM

m	n_λ	N_h	N_{Σ_h}	BGT	Padé ($\pi/6, 2$)	Padé ($\pi/3, 2$)
1(C)	10	65153	888	5.42(14.23)	5.46(14.23)	5.46(14.22)
	20	224151	1776	1.48(3.74)	1.40(3.66)	1.40(3.67)
	40	1034390	3551	0.74(1.18)	0.48(0.98)	0.47(0.99)
0.125	10	4644	604	16.19(18.45)	9.75(13.87)	10.08(15.04)
	20	18051	1206	16.47(16.51)	8.21(8.32)	7.81(8.29)
	40	69959	2416	16.54(16.54)	8.83(8.80)	8.32(8.32)
0.25	10	5605	614	14.77(17.41)	7.91(12.52)	8.98(14.07)
	20	21190	1230	14.20(14.67)	6.87(7.03)	6.48(7.14)
	40	83679	2456	14.67(14.55)	7.48(7.43)	6.95(7.00)
0.5	10	7222	634	12.03(18.50)	9.01(13.78)	9.24(14.83)
	20	28557	1268	12.70(14.15)	5.68(6.68)	5.79(7.14)
	40	112690	2536	13.25(13.58)	6.32(6.48)	6.30(6.54)
1	10	11054	672	10.20(19.07)	7.88(14.65)	8.74(14.91)
	20	43857	1346	11.50(13.58)	4.45(6.04)	3.95(5.89)
	40	173154	2694	12.05(12.54)	4.45(4.81)	4.68(4.94)

REFERENCES

1. O.C. Zienkiewicz, Achievements and some unsolved problems of the finite element method, *International Journal for Numerical Methods in Engineering* **47** (200), pp.9-28.
2. D. Colton and R. Kress, *Integral Equation Methods in Scattering Theory*, Pure and Applied Mathematics, John Wiley and Sons, Inc., New York, 1983.
3. V. Rokhlin, Rapid solution of integral equations of scattering theory in two-dimensions, *Journal of Computational Physics* **186** (1990), pp.414-439.
4. O.P. Bruno and L.A. Kunyansky, A fast, high-order algorithm for the solution of surface scattering problems: basic implementation, tests, and applications, *Journal of Computational Physics* **169** (1), (2001), pp.80-110.
5. O.P. Bruno and L.A. Kunyansky, Surface scattering in three dimensions: an accelerated high-order solver, *P. R. Soc. Lond. Proc. Ser. A Math. Phys. Eng. Sci.* **457** (2016) (2001), pp. 2921-2934.
6. X. Antoine and M. Darbas, Alternative Integral Equations for the Iterative Solution of Acoustic Scattering Problems, *Quarterly Journal of Mechanics and Applied Mathematics*, (in press, 2005).
7. J.C.Nédélec, *Acoustic and Electromagnetic Equations, Integral Representations for Harmonic Problems*, Applied Mathematical Sciences, 144 Springer-Verlag, New York, 2001.
8. I. Harari, K. Gosh, T.J.R. Hughes, M. Malhotra, P.M. Pinsky, J.R. Stewart, L.L. Thompson, Recent developments in finite element methods for structural acoustics, *Archiv. Comput. Methods Eng.* **3** (2 y 3) (1996) 131311.
9. I. Harari and F. Magoules, Numerical investigations of stabilized finite element computations for acoustics, *Wave Motion* **39** (4), pp. 339-349 (2004).
10. R. Djellouli, C. Farhat, A. Macebo and R. Tezaur, Finite element solution of two-dimensional acoustic scattering problems using arbitrarily-shaped convex artificial boundaries, *Journal of Computational Acoustics* **8** (2000), pp.81-100.
11. R. Tezaur, A. Macedo, C. Farhat and R. Djellouli, Three-dimensional finite element calculations in acoustic scattering using arbitrarily-shaped convex artificial boundaries, *International Journal for Numerical Methods in Engineering* **53** (2002), pp.1461-1476.
12. A. Bayliss, M. Gunzburger, E. Turkel, Boundary conditions for the numerical solution of elliptic equations in exterior regions, *SIAM Journal of Applied Mathematics* **42** (1982) 430-451.
13. A. Bayliss, E. Turkel, Radiation boundary conditions for wave-like equations, *Communications on Pure and Applied Mathematics* **33** (6) (1980) 707-725.
14. J.P. Bérenger, A perfectly matched layer for the absorption of electromagnetic waves, *Journal of Computational Physics* **114** (1994) 185-200.
15. D. Givoli, Exact representation on artificial interfaces and applications in mechanics, *Appl. Mech. Rev.* **52**

- (1999) 333-349.
16. T. Hagstrom, Radiation boundary conditions for the numerical simulation of waves, *Acta Numerica* (1999) 47-106.
 17. R. Kechroud, A. Soulaïmani, Y. Saad and S. Gowda, Preconditioning techniques for the solution of the Helmholtz equation by the finite element method, *Mathematics and Computer in Simulation* 65 (2004), no. 4-5, 303-321.
 18. S.V. Tsynkov, Numerical solution of problems on unbounded domains, A review, *Applied Numerical Mathematics* 27 (1998) 465-532.
 19. F. Ihlenburg, *Finite Element Analysis of Acoustic Scattering*, Springer, New York, 1998.
 20. Y. Saad, *Iterative Methods for Sparse Linear Systems*, PWS Pub. Co., Boston, 1996.
 21. B. Engquist and A. Majda, Absorbing boundary conditions for the numerical simulation of waves, *Mathematics of Computation* 31 (1977), pp. 629-651.
 22. X. Antoine, M. Darbas and Y.Y. Lu, An Improved Surface Radiation Condition for High-Frequency Acoustics Scattering Problems, submitted (2004).
 23. F.A. Milinazzo, C.A. Zala, G.H. Brooke, Rational square-root approximations for parabolic equation algorithms, *Journal of the Acoustical Society of America* 101 (2) (1997) 760-766.
 24. X. Antoine, H. Barucq and A. Bendali, Bayliss-Turkel-like radiation conditions on surfaces of arbitrary shape, *Journal of Mathematical Analysis and Applications* 229 (1999), pp.184-211.
 25. C. Farhat, R. Tezaur and R. Djellouli, On the solution of three-dimensional inverse obstacle acoustic scattering problems by a regularized Newton method, *Inverse Problems* 18 (2002), no. 5, pp. 1229-1246.
 26. C. Farhat and U. Hetmaniuk, A fictitious domain decomposition method for the solution of partially axisymmetric acoustic scattering problems. I. Dirichlet boundary conditions, *International Journal for Numerical Methods in Engineering* 54 (2002), no. 9, pp. 1309-1332.
 27. U. Hetmaniuk, and C. Farhat, A fictitious domain decomposition method for the solution of partially axisymmetric acoustic scattering problems. II. Neumann boundary conditions, *International Journal for Numerical Methods in Engineering* 58 (2003), no. 1, pp. 63-81.
 28. X. Antoine, Fast Approximate computation of a time-harmonic scattered field using the on-surface radiation condition method, *IMA Journal of Applied Mathematics* 66 (2001) pp. 83-110.
 29. I. Harari and R. Djellouli, Analytical study of the effect of wave number on the performance of local absorbing boundary conditions for acoustic scattering, *Applied Numerical Mathematics* 50 (2004) 15-47.
 30. D. Givoli, High-order local non-reflecting boundary conditions: a review, *Wave Motion* 39 (2004) 319-326.
 31. M.N. Guddati and J.L. Tassoulas, Continued-fraction absorbing boundary conditions for the wave equation, *Journal of Computational Acoustics* 8 (1) (2000) 139-156.
 32. L.L. Thompson, R. Huan and D. He, Accurate radiation boundary conditions for the two-dimensional wave equation on unbounded domains, *Comput. Methods Appl. Mech. Engrg.* 191 (2001) 311-351.
 33. X. Antoine, An Algorithm Coupling the OSRC and FEM for the Computation of an Approximate Scattered Acoustic Field by a Non-convex Body, *International Journal for Numerical Methods in Engineering* 54 (7) (2002), pp. 1021-1041.
 34. G.A. Kriegsmann, A. Taflove, K.R. Umashankar, A new formulation of electromagnetic wave scattering using the on-surface radiation condition method, *IEEE Transactions on Antennas and Propagation* 35 (1987) 153-161.
 35. M. Taylor, *Pseudodifferential Operators*, Princeton University Press, Princeton, NJ, 1981.
 36. L. Little, Y. Saad, L. Smoch, Block LU preconditioners for symmetric and nonsymmetric saddle point problems, *SIAM J. Sci. Comput.* 25 (2), (2003), pp. 729-748.
 37. S. Kirkup, The boundary element method in acoustics. A development in Fortran, *Integral Equation Methods in Engineering*, 1. Integrated Sound Software, Hebden Bridge, 1998. The code is available at: <http://www.boundary-element-method.com/>.
 38. I. Harari and C.L. Carnot, Reducing dispersion of linear triangular elements for the Helmholtz equation, *Journal of Engineering Mechanics*, March 2002 351-258.
 39. O. Vacus, Mathematical analysis of absorbing boundary conditions for the wave equation: the corner problem, *Mathematics of Computation*, 74 (249), (2005), pp.177-200 .
 40. M. Darbas, *Préconditionneurs Analytiques de Type Caldéron pour les Formulations Intégrales des Problèmes de Diffraction d'Ondes*, Ph. Thesis, Université de Toulouse, December 2004.